



# Mangrove Growth Monitoring Based on Camera Visible Images—A Case Study on Typical Mangroves in Guangxi

Yanli Chen<sup>1,2</sup>, Shibo Fang<sup>3\*</sup>, Ming Sun<sup>2</sup>, Zhiping Liu<sup>2</sup>, Lianghao Pan<sup>1</sup>, Weihua Mo<sup>2</sup> and Cheng Chen<sup>2</sup>

<sup>1</sup>Guangxi Key Lab of Mangrove Conservation and Utilization, Guangxi Mangrove Research Center, Guangxi Academy of Sciences, Beihai, China, <sup>2</sup>Guangxi Institute of Meteorological Sciences, Nanning, China, <sup>3</sup>State Key Laboratory of Severe Weather, Chinese Academy of Meteorological Sciences, Beijing, China

## OPEN ACCESS

### Edited by:

Chuang Zhao,  
China Agricultural University, China

### Reviewed by:

Costica Nitu,  
Politehnica University of Bucharest,  
Romania  
Muhammad Kamal,  
Gadjah Mada University, Indonesia

### \*Correspondence:

Shibo Fang  
sbfang0110@163.com

### Specialty section:

This article was submitted to  
Environmental Informatics and Remote  
Sensing,  
a section of the journal  
Frontiers in Earth Science

**Received:** 07 September 2021

**Accepted:** 15 December 2021

**Published:** 17 February 2022

### Citation:

Chen Y, Fang S, Sun M, Liu Z, Pan L,  
Mo W and Chen C (2022) Mangrove  
Growth Monitoring Based on Camera  
Visible Images—A Case Study on  
Typical Mangroves in Guangxi.  
*Front. Earth Sci.* 9:771753.  
doi: 10.3389/feart.2021.771753

Mangroves are an important coastal wetland ecosystem, and the high-throughput visible light (RGB) images of the canopy obtained by the ecological meteorological station can provide basic data for quantitative and continuous growth monitoring of mangroves. However, as for the mangroves that are subject to periodic seawater submersion, some key technical issues such as image selection, vegetation segmentation, and index applicability remain unsolved. With the typical mangroves in Beihai, Guangxi, as the object in this study, we used canopy RGB images and tidal data to find out the screening methods for high-quality nontidal submerged images, as well as the vegetation segmentation algorithms and RGB vegetation index applicability, so as to provide technical reference for the use of RGB images to monitor mangrove growth. The results showed that: 1) The critical tide levels can be determined according to the periodic changes of submersion in the mangroves, and critical tidal levels and image brightness can be used to quickly screen high-quality images of mangroves that are not submerged by seawater. 2) Machine learning and NLM filtering are effective strategies to obtain high-precision mangrove segmentation results. The machine learning algorithm has superiority in the segmentation of mangrove vegetation with a segmentation accuracy of higher than 80%, and the nonlocal mean filtering can effectively optimize the segmentation results of various algorithms. 3) The seasonal index VEG and antiseasonal index CIVE can be used as the optimal indices for mangrove growth monitoring, and the compound sine function can better simulate the change trend of various RGB vegetation indices, which is convenient for quickly judging mangrove growth changes. 4) Mangrove RGB vegetation indices are sensitive to meteorological factors and can be used to analyze the influence of meteorological conditions on mangrove growth.

**Keywords:** mangroves, visible image, image segmentation, machine learning, nonlocal mean filtering

## 1 INTRODUCTION

As a special ecosystem at the land–sea interface, mangroves encompass both important ecological service functions and socioeconomic values (Zhu et al., 2014). It can play an important role in wind and wave defense, pollution prevention, and beautification of the coast. Quantitative monitoring of mangrove growth conditions can provide an important data basis for in-depth interpretation of mangrove ecosystem functions. As the mangroves that grow on the intertidal zone of the coast or at the mouth of the river are subject to periodic tidal submersion (Zhang and Zheng, 1997), there are some problems in the traditional field sampling growth survey, such as lack of representativeness, and it is difficult for investigators to enter the mangrove growth area (Wen et al., 2020). Satellite remote sensing technology provides a convenient means for mangrove growth monitoring. The leaf area index (Ramsy and Jensen, 1996; Kovacs et al., 2005) and normalized vegetation index (Cao, 2017) retrieved by remote sensing can be used for mangrove health monitoring. However, due to the satellite revisit cycle and cloud and rain weather, it is difficult to ensure the continuity of high-resolution satellite remote sensing data suitable for mangrove growth monitoring (Zhang, 2016; Zhu et al., 2020). Thus, both traditional ground survey and satellite remote sensing technology have some problems, such as lack and incompleteness of key information, which is difficult to be used for quantitative and continuous monitoring of mangrove growth.

In recent years, the widespread construction of ecological meteorological observatories in China has made camera visible light (RGB) images become normalized data. As an important part of the space–air–ground integrated monitoring network, this type of data can be an effective supplement to satellite remote sensing and UAV remote sensing, making it able to achieve the high-throughput time-series monitoring of vegetation growth. Guangxi established a mangrove ecological meteorological observation station in 2018, providing important basic data for mangrove growth monitoring. However, the current key technologies of RGB images are mainly applied to crops, and it has been proven that the technologies can effectively monitor the growth period (Lu et al., 2011; Wu, 2014; Wu et al., 2018; Liu et al., 2020), coverage (Purcell, 2000; Campillo et al., 2008; Yang et al., 2018), growth vigor (Zhou et al., 2015; Han et al., 2019), and nitrogen status (Chen et al., 2017; Shi et al., 2020) of crops. Although UAV RGB images have achieved initial success in mangrove vegetation segmentation and canopy structure inversion (Jones et al., 2020; Wen et al., 2020), whether the RGB images acquired by the ground are effective in monitoring mangrove growth conditions remains to be clarified. Moreover, some key issues related with image selection, vegetation segmentation, and index applicability for mangroves, which are subject to periodic seawater submersion, are still rarely reported.

Image selection is the primary problem to be solved to apply RGB images in mangrove monitoring. Mostly shot in fixed time and fixed angle in the station, the canopy images can be obtained at multiple times in a day. Long-term sequence monitoring

involves the screening of a large number of image data. Therefore, for mangroves, first of all, it is necessary to ensure that the selected images are not affected by seawater submersion. Under the effect of tides, the rise and fall of seawater change, and the submerging time of mangroves in different regions is also different (Zhang and Zheng, 1997), which brings difficulties to the selection of mangrove canopy images. In addition, the quality of the obtained canopy image will be different due to the influence of light conditions. Therefore, the selection of mangrove canopy images involves two issues: analysis of tidal submerging rules and judgment of image brightness.

Vegetation segmentation is a key technology in using RGB images to carry out mangrove monitoring. Image segmentation aims to divide the images containing the spatial distribution information of complex surface features into different regions with specific semantic labels (Min et al., 2020), which is the basis for vegetation monitoring using near-ground canopy RGB images. Currently, the developed segmentation methods include area (Liu et al., 2021), histogram thresholding (Chen et al., 2011), feature space clustering (Li et al., 2020), edge detection (Ren et al., 2004), fuzzy technology (Ma et al., 2008), artificial neural network (Ma et al., 2020), and deep learning (Yan et al., 2021). At present, these segmentation algorithms have been successfully applied in crops, but there has been no report on the application in mangroves.

The selection of monitoring index is the basis for the quantitative monitoring and evaluation of mangrove growth. At present, scholars have constructed various RGB vegetation indices to monitor the changes in crop growth, namely, NDYI (normalized difference yellowness index) (Sulik and Long, 2016), GLA (green leaf algorithm) (Guijarro et al., 2011), VARI (visible atmospherically resistant index) (Gitelson et al., 2002), and NGRDI (normalized green–red difference index) (Pérez et al., 2000). However, due to the wavebands and parameter composition, the developed indices are mostly for crops, and the applicability of these indices in mangrove growth monitoring also needs to be reassessed.

The objective of this study was to demonstrate the plausibility of monitoring and evaluating the canopy growth of mangrove using the existing RGB image processing technology. To achieve this objective, we performed the analysis on the screening method of high-quality nontidal submerging images, developed the high-precision segmentation algorithm of mangrove vegetation, and applied RGB image-based vegetation indices to monitor mangrove growth. This study provides technical references for the application of RGB images in the rapid and accurate monitoring of mangrove growth.

## 2 DATA AND METHODS

### 2.1 Study area

Completed at the end of 2018, the Beihai Mangrove Ecological Meteorological Observatory is located in the small bay (21°27'5.57"N, 109°18'4.39"E) of the National Marine Science and Technology Park in Beihai City, Guangxi. The geographical location is shown in **Figure 1**. The study area has a subtropical

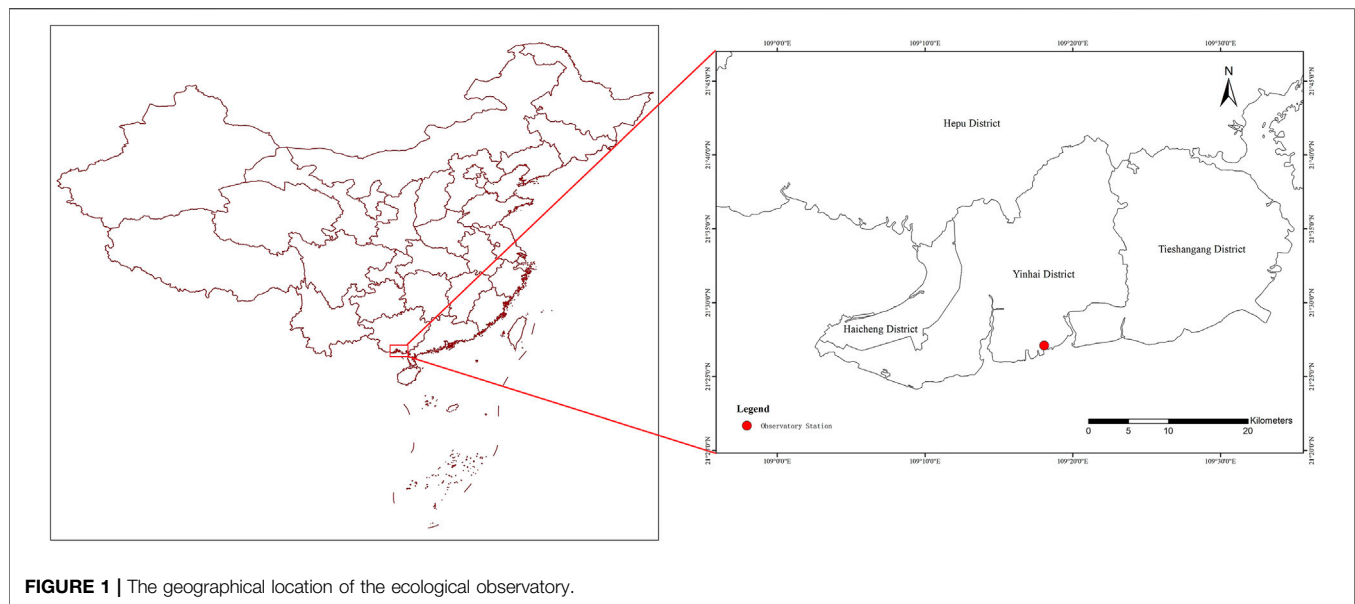


**FIGURE 1** | The geographical location of the ecological observatory.

monsoon climate, warm and humid throughout the year, with an average annual rainfall of 1,644.0 mm and an average annual temperature of 22.6°C. The mangrove forest in the study area has a total area of about 5.5 hm<sup>2</sup>, where the species is dominated by the *Aricennia marina* community, mixed with some *Kandelia obovata* and *Aegiceras corniculata*. The soil is mainly composed of fine gravel sand to coarse sand, which has low organic matter content.

## 2.2 Data

### 2.2.1 RGB images

The RGB images were taken from the digital camera erected on the flux tower of the ecological meteorological observatory. The camera was erected at 6 m above the ground. The camera model is ZQZ-TIM, and it uses a 1/1.8 inch CMOS sensor with the total pixels of about 6.44 million, aperture value of F1.5-4.3, 30 times optical zoom, 16 times digital zoom, wide dynamic effect, plus image noise reduction function, all of which enable it to better display day/night images. Moreover, the camera can achieve continuous monitoring with 360° continuous rotation in the horizontal direction, continuous monitoring after -20°-90° autoflip to 180° in the vertical direction, which has no blind spot monitoring. After acquisition, the images can be uploaded to the cloud platform or imported into the computer for processing. The RGB images were collected from 8:00 to 17:00 every day, with an interval of 1 h, and the image sequence time period was from September 3, 2018 to August 31, 2019.

### 2.2.2 Meteorological and tidal data

The meteorological data was collected from the automatic meteorological observation equipment of the ecological meteorological observatory. The observation elements included daily average temperature, daily maximum temperature, daily minimum temperature, relative humidity, and precipitation. The tidal data came from the Chinese Tide Table (Beihai port)

compiled by the China Oceanic Information Center, and the observation elements included the tidal levels in every hour, time of tide, and tidal levels. These data were combined with RGB images to analyze the critical tidal levels when mangroves were submerged in seawater.

## 2.3 Research methods

### 2.3.1 RGB image selection

Image selection is to reduce the impact of tidal submersion, cloud covering, and illumination changes on the image quality of mangrove canopy, so as to obtain better images for vegetation segmentation and index calculation. First, the critical tidal level of seawater submersion in the study area was determined through the combination of visual interpretation and tidal data. Then the visual images with lower tidal levels were screened out. Finally, the image with the highest brightness was selected as the image of the day. During the process, the brightness of the visible images was represented by the sum of the R, G, and B color channel values (Peter et al., 2018). The critical tidal levels of the mangroves in the study area were determined as follows: 1) Randomly select the visible image data set with seawater submersion for 3 days every month. 2) Find the images with a small amount of water or completely exposed mud flat after comparing the submerging status in the mud flat on the images, and use the shooting time of the image as the time when the tide begins to rise or finishes falling. 3) Determine the critical tidal level according to the tide table at that time.

### 2.3.2 RGB image segmentation

The purpose of image segmentation is to accurately obtain green vegetation information from the entire image. In order to find a better segmentation algorithm for mangrove vegetation, we compared the accuracy of three different types of segmentation algorithms. The first algorithm used the individual channel of color space as the input of the Ostu

threshold segmentation algorithm (Ostu, 1979) to achieve the automatic segmentation of vegetation. For example, there is a significant difference in the S channel in HSV space and in a channel in lab space between vegetation and background in RGB images, and values of these two channels both showed bimodal distribution in the image, providing the basis of automatic segmentation. The second used the nonlinear calculation by combining values of different channels, which enhanced proportion of green components and showed significant difference and pattern between vegetation and background in RGB images. A widely used and proven color index ExG was applied to discriminate vegetation from non-vegetation part in this study. The third segmentation algorithm that is based on machine learning took advantage of training classifiers with multidimensional classification samples to utilize rich information by mapping indistinguishable problems at low dimension to a high dimension. The K-means unsupervised clustering was first performed to generate training samples that were divided into vegetation, dark background, and bright background. Then features of vegetation pixels including 24 indexes from the dimension of color, texture, and gradient were extracted from the training samples to generate classification feature vectors. The support vector machine (SVM) was then used to classify vegetation and background in images.

Affected by factors such as differences in lighting conditions and imaging quality, it is fairly probable for the marginal part of vegetation to be wrongly segmented. In order to reduce the erroneous segmentation of leaf edges, nonlocal means (NLM) was introduced to optimize the results of vegetation segmentation. The NLM operator can protect the long and narrow structure similar to the vegetation leaf, and eliminate the ambiguity of pixel segmentation at the edge of the vegetation leaf by enhancing the nonadjacent pixels on the same structure within a certain neighborhood. The principle of the NLM algorithm is as follows:

Assume that the noising image is  $v = \{v(a) | a \in A\}$ , the image after denoising is  $NL[v]$ , then the weighted value of each pixel  $a$  can be calculated by the following formula:

$$NL[v](a) = \frac{1}{C(a)} \sum_{b \in I} w(a, b) v(b)$$

where  $w(a, b)$ , is the weight of the similarity between pixel  $a$  and pixel  $b$  (Gaussian weighted Euclidean distance), which meets the requirement of  $0 \leq w(a, b) \leq 1$  and  $\sum_b w(a, b) = 1 \quad 0 \leq a \leq 1$ . The formula is as follows:

$$w(a, b) = \frac{1}{C(a)} \exp\left(-\frac{\|v(N(a)) - v(N(b))\|_{2,a}^2}{h^2}\right)$$

$$C(a) = \sum_{b \in I} \exp\left(-\frac{\|v(N(a)) - v(N(b))\|_{2,a}^2}{h^2}\right)$$

where  $\|v(N(a)) - v(N(b))\|_2^2$  is the square of the Gaussian weighted distance between the pixel in the subblock centered on pixel  $a$  and the pixel in the subblock centered on pixel  $b$ , which is used to measure the similarity between two pixels;  $a$  is the

standard deviation,  $v(N(a))$  is the set of local sub-block pixels around  $a$ ; and  $h$  is the filter parameter.

The onsite labeling results were used as reference to evaluate the accuracy of the classified images obtained before and after the filtering of the above three segmentation algorithms. The accuracy evaluation indicators  $Q_{seg}$  and  $S_r$  are calculated as follows:

$$Q_{seg} = \frac{\sum_{i=0}^{i=m} \sum_{j=0}^{j=n} (A(p)_{ij} \cap B(p)_{ij})}{\sum_{i=0}^{i=m} \sum_{j=0}^{j=n} (A(p)_{ij} \cup B(p)_{ij})}$$

$$S_r = \frac{\sum_{i=0}^{i=m} \sum_{j=0}^{j=n} (A(p)_{ij} \cap B(p)_{ij})}{\sum_{i=0}^{i=m} \sum_{j=0}^{j=n} B(p)_{ij}}$$

where,  $A$  is the foreground (green vegetation) pixel set ( $p = 255$ ) or background (information other than green vegetation) pixel set ( $p = 0$ ) of the segmented image,  $B$  is the foreground pixel set obtained by field labeling ( $p = 255$ ) or background pixel set ( $p = 0$ ),  $m$  and  $n$  are the number of lines and columns of the image, respectively, and  $i$  and  $j$  are the corresponding coordinates, respectively. The larger the  $Q_{seg}$  and  $S_r$  values indicate higher segmentation accuracy.  $Q_{seg}$  is the overall consistency of the background and foreground segmentation results, while  $S_r$  only represents the consistency of the foreground segmentation result.

### 2.3.3 Calculation and simulation RGB vegetation indices

The calculation of RGB vegetation indices is as follows: After the segmentation of the green vegetation in the visible image, the R, G, and B color channel values of each pixel in the green vegetation area were extracted, then all the pixels in the area were averaged, and finally, the visible vegetation indices of mangroves were calculated (Table 1).

Vegetation change trend was simulated as follows: the compound sine function was used to simulate the change trend of mangrove growth over time, which was mainly used for quick judgment of mangrove growth. The calculation formula is as follows:

$$VI = a + b \sin\left[\frac{2\pi(t_{day} - c)}{365}\right]$$

where,  $a$ ,  $b$ , and  $c$  are all empirical coefficients, and  $t_{day}$  is the day order.

The change rules of the various indices and the simulation results of vegetation change trend were compared to analyze the applicability of RGB vegetation indices for mangrove monitoring.

## 3 RESULT ANALYSIS

### 3.1 Fast screening of mangrove images

Affected by the tidal force of different cycles and the topography of the coastal zone, the tidal levels of the sea area presented a complex periodic movement over time. According to the submerging degrees classified by Zhang and Zheng, (1997), the



**TABLE 1 |** RGB vegetation indices.

Image index	Calculation formula	Source
NDYI	$NDYI = (G - B) / (G + B)$	Sulik and Long,(2016)
GLA	$GLA = (2G - R - B) / (2G + R + B)$	Guijarro et al.,(2011)
VARI	$VARI = (G - R) / (G + R - B)$	Gitelson et al.,(2002)
ExG	$ExG = 2g - r - b$	Woebbecke et al.,(1995)
ExR	$ExR = 1.4r - g$	Meyer et al.,(1999)
MGRVI	$MGRVI = (g^2 - r^2) / (g^2 + r^2)$	Bendig et al.,(2015)
RGBVI	$RGBVI = (g^2 - br) / (g^2 + br)$	Bendig et al.,(2015)
NGRDI	$NGRDI = (G - R) / (G + R)$	Pérez et al.,(2000)
CIVE	$CIVE = 0.441r - 0.811g + 0.385b + 18.78745$	Kataoka et al.,(2003)
VEG	$VEG = g / (r^{0.667} b^{0.333})$	Hague et al.,(2006)

Note. R, G, B are the red, green, and blue band values, respectively; r, g, b are the normalized red, green, and blue band values.

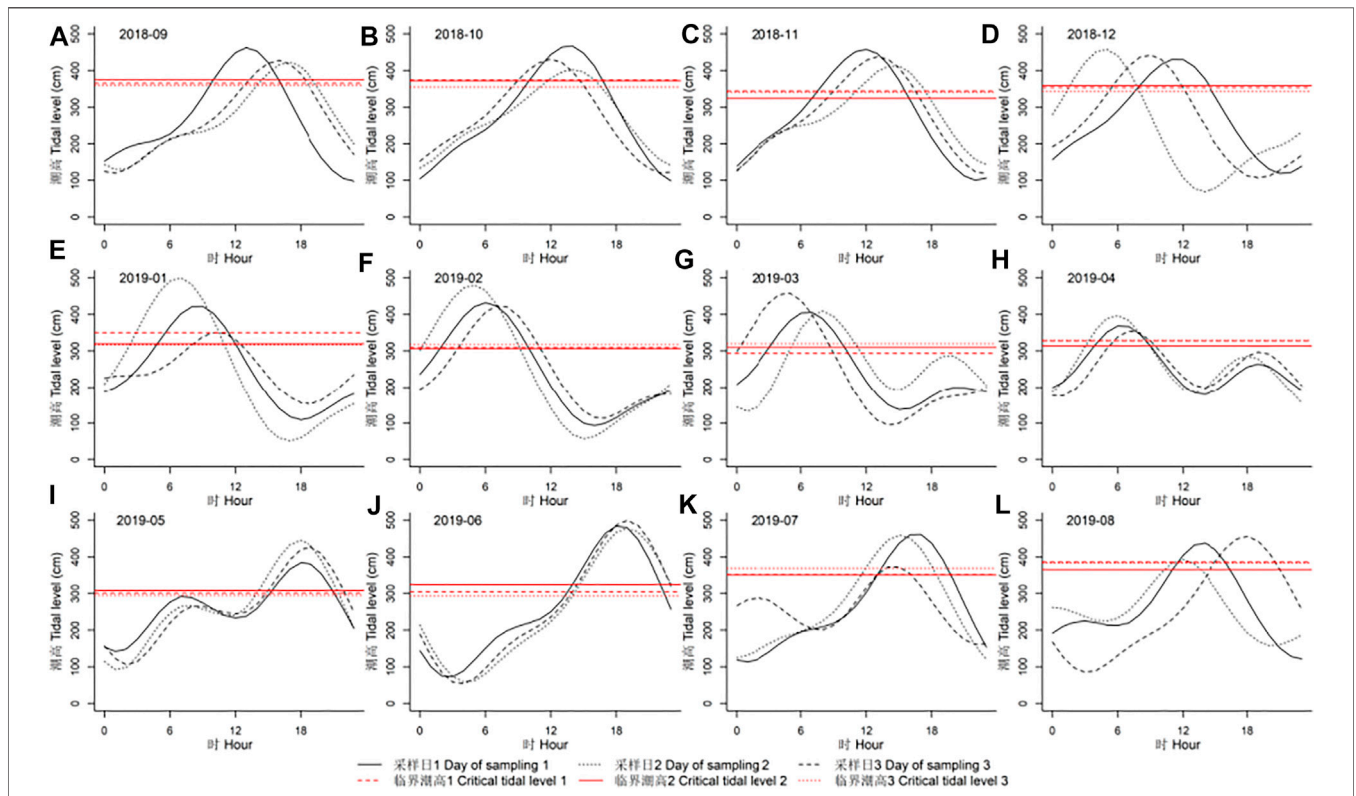


**FIGURE 2 | (A)** The distribution of tidal levels and critical tidal levels in mangrove vegetation areas from September 2018 to August 2019.

mangroves at the study area were at once-a-day short-term submerging degree. The start time of submersion all presented a cyclical change with the passage of time, which was delayed first and then shifted to an earlier time. From January to April, tidal submersion all began in the wee hours and ended in the morning; from May to August, tidal submersion began in the afternoon and ended at night; and from September to December, the beginning of tidal submersion gradually shifted from noon to the morning and even to the wee hours, and then ended in the afternoon. The annual average critical tidal level of the mangroves at the study area is 334.8 cm, with a maximum of 376 cm and a minimum of 294 cm (Figure 2). Therefore, in this study, the visual images with

tidal levels of lower than 294.0 cm were selected for image segmentation and vegetation index calculation, which could ensure the least effects caused by tidal submersion.

### 3.1 Applicable algorithms for mangrove vegetation segmentation

Visual interpretation found that different segmentation algorithms had significant differences in sensitivity to mangroves and background information. The algorithms based on color space, nonlinear combination of color channels, and machine learning could highly distinguish the bright green

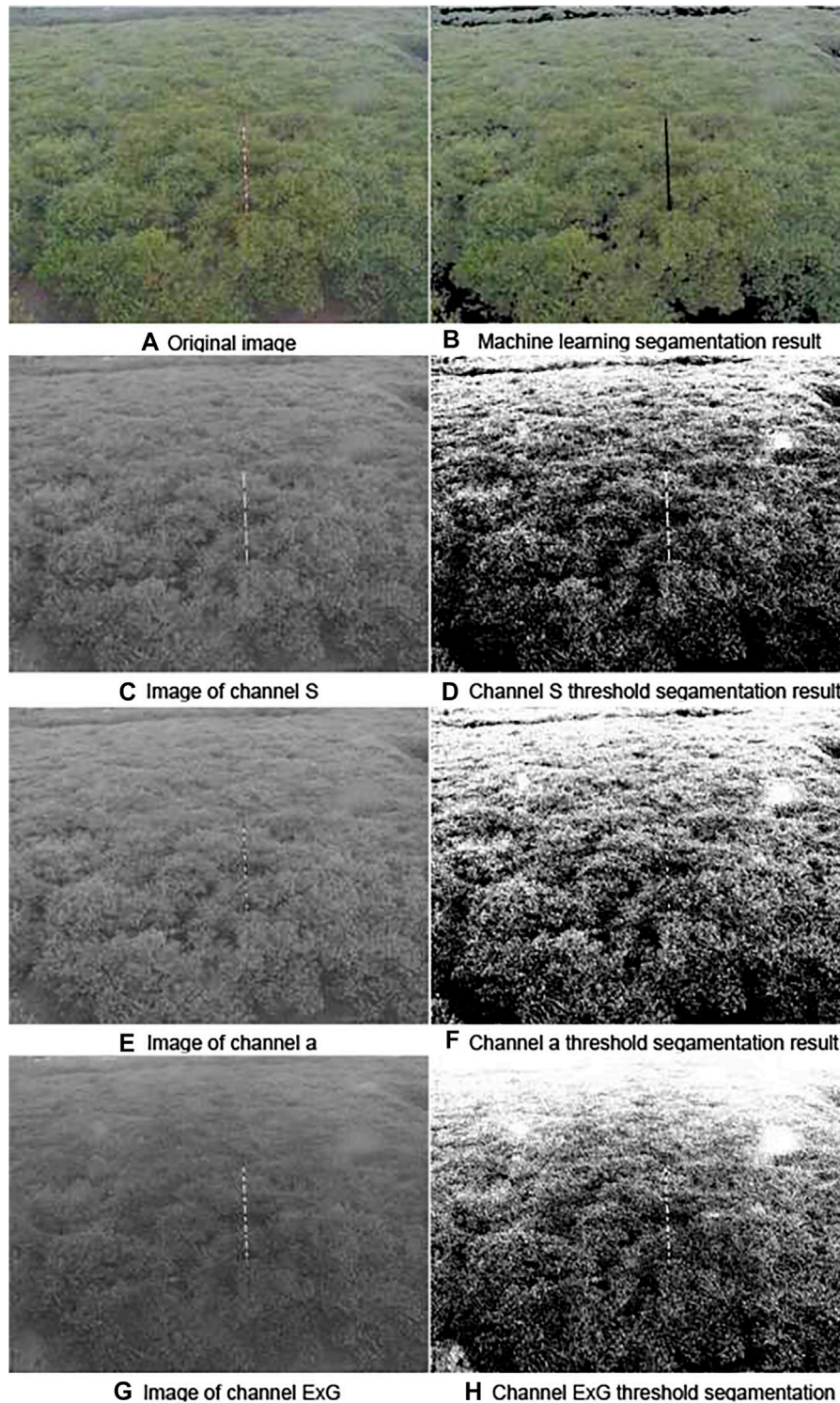


**FIGURE 3 |** Segmentation effects of mangrove vegetation images. **(A)** Original image. **(B)** Machine learning segmentation result. **(C)** Image of channel S. **(D)** Channel S threshold segmentation result. **(E)** Image of channel a. **(F)** Channel a threshold segmentation result. **(G)** Image of channel ExG. **(H)** Channel ExG threshold segmentation.

**TABLE 2** | Comparison on accuracy of mangrove vegetation image segmentation algorithms.

—		Channel a (%)	Channel S (%)	ExG (%)	Machine learning (%)
No filter	Qseg	75.32	76.27	73.60	80.56
	Sr	77.39	79.58	75.45	86.46
After filtering	Qseg	76.19	77.36	74.64	81.70
	Sr	78.80	81.02	77.06	87.27

mangroves in the close-range view, and the differences in segmentation results were not significant. However, differences became significant when using the algorithms to distinguish the mud flat in close-range view and grayish-green mangroves in distant-range view, which were in the order of machine learning > channel S > channel a > ExG (Figure 3).

The accuracy of machine learning algorithm for segmentation of mangrove vegetation was better than other algorithms. Machine learning also showed the best segmentation effect when using field labeling results as a reference to quantitatively analyze the segmentation accuracy of the three kinds of algorithms, with the *Qseg* and *Sr* of 80.56% and 86.46%, respectively, and the accuracy rates of other segmentation algorithms were lower than 80%, of which EXG showed the poorest segmentation effect with the *Qseg* and *Sr* of 73.60% and 75.45%, respectively (Table 1).

NLM filtering could effectively optimize various segmentation results. After filtering processing, the error segmentation of background information, such as mangrove leaf edges and mudflats, were significantly reduced, with an *Qseg* increase of 0.88%–1.15% and *Sr* increase of 0.81%–1.61%. The optimization effect was the most significant on the segmentation results of channel S, and the accuracy was improved the most after filtering. Considering the overall performances, machine learning was used for the original RGB image segmentation and NLM filtering optimization strategy. In this way, the final segmentation accuracy of mangrove vegetation could reach 87.27% (Table 2).

### 3.3 Applicable monitoring index for mangrove growth monitoring

The 10 RGB vegetation indices could be divided into two categories according to their sequential variation characteristics. The first category contained the indices with seasonal changes that were quasisynchronous with temperature changes (collectively referred to as seasonal indices), including ExG, ExGR, GLA, GMRVI, NDYI, RGBVI, VARI, and VEG. The indices in this category have lower values in winter and spring, while they have higher values in summer and autumn. The second category was the indices with seasonal change trend that was opposite to the temperature change over time (collectively referred to as the antiseasonal indices), including ExR and CIVE. The indices in this category had lower values in summer and autumn, but higher values in winter and spring, which was opposite to the seasonal indices (Figure 4).

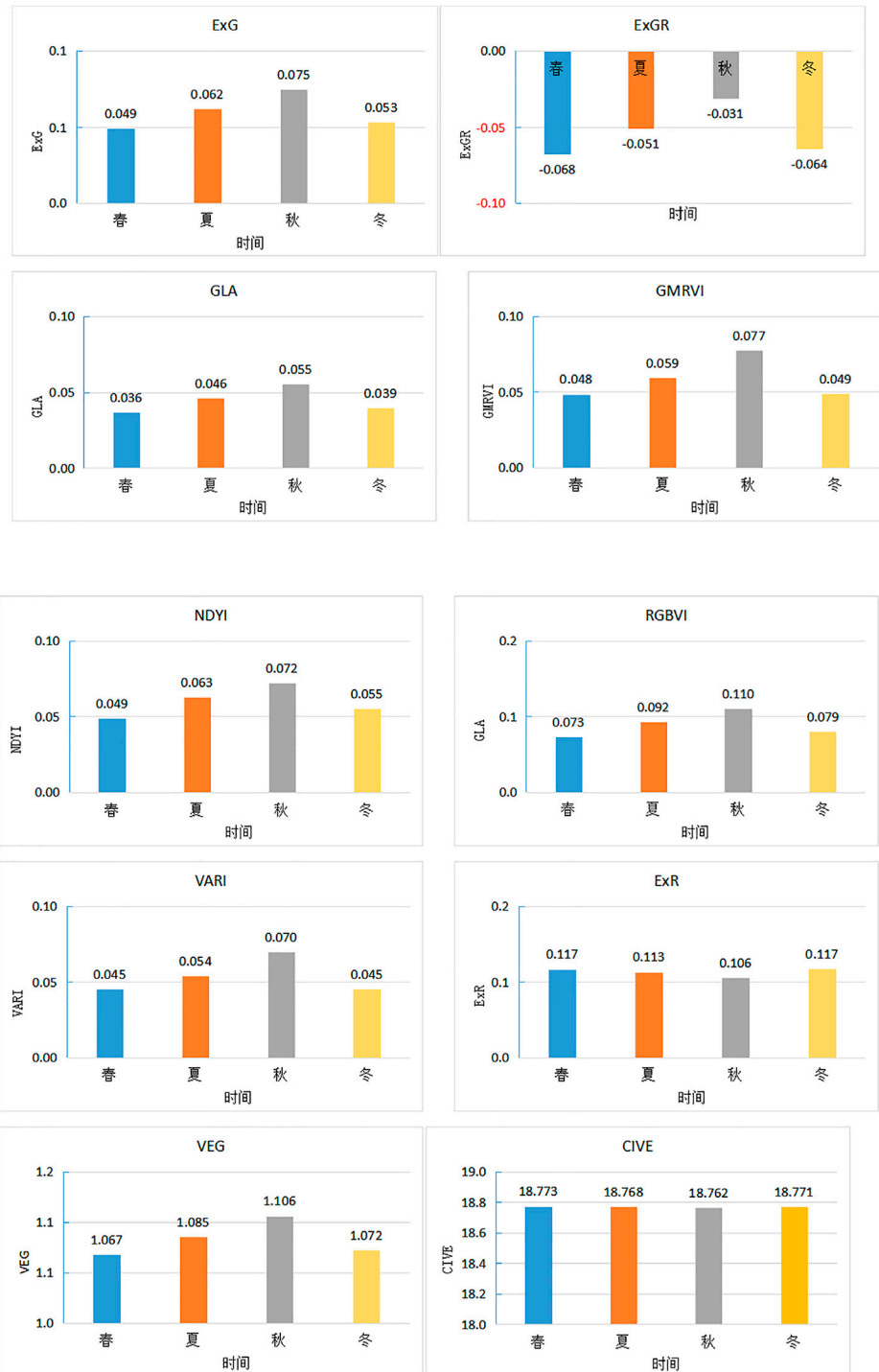
Compound sine function could better simulate the periodic changes in various RGB vegetation indices during the year. The correlation coefficients between the simulated and observed

values of various indices were between 0.430 and 0.643, among which VARI had the best fitting effect ( $R = 0.643$ ), and ExG had the worst fitting effect ( $R = 0.505$ ). The annual sequence fitting deviations of various indices were between 0.03% and 26.16%, among which ExR (4.09%), VEG (1.73%), and CIVE (0.03%) showed relatively small deviations between the fitted values and observed values, while the deviations of other indices were all greater than 17% (Figure 5; Table 3).

The simulated results of various RGB vegetation indices fitted by the compound sine function showed significant differences in seasons. The deviation was 0.02%–17.98% in spring, 0.04%–39.97% in summer, 0.05%–59.66% in autumn, and 0.02%–22.05% in winter. In comparison, the deviations were small in winter and spring, and large in summer and autumn (Table 3). Therefore, seasonal index VEG and antiseasonal index CIVE could be used as the preferred indices for mangrove growth monitoring. The reasons were that, as one of the seasonal indices, VEG made it easier to understand the impact of weather conditions on mangrove growth, while CIVE, an antiseason index, had smaller simulation deviation.

### 3.4 Response of mangrove growth monitoring indices to meteorological factors

The selected main meteorological factors were daily average temperature, daily maximum temperature, daily minimum temperature, relative humidity, and daily precipitation, which were used to make correlation analysis with mangrove canopy RGB vegetation indices (Table 4). There was a high degree of correlation among various RGB vegetation indices (Table 5), but due to the difference in image bands and parameters, the correlations between different RGB vegetation indices and meteorological factors were significantly different. The eight seasonal RGB vegetation indices (ExG, ExGR, GLA, GMRVI, NDYI, RGBVI, VARI, and VEG) were positively correlated with average temperature, maximum temperature, minimum temperature, and precipitation, and negatively correlated with relative humidity, while the correlations between the two counterseasonal RGB vegetation indices (ExR and CIVE) and the meteorological factors were opposite to those of the seasonal indices. Among them, ExR, VARI, GMRVI, and NGRDI showed significant correlations with temperature (average, maximum, and minimum) and relative humidity, while NDYI and CIVE showed no significant correlation with temperature and relative humidity. In terms of precipitation, the correlation with NDYI, GLA, RGBVI, CIVE, and VEG reached significant levels, while the other RGB vegetation indices were not significantly



春=Spring 夏=Summer 秋=Autumn 冬= Winter 时间=time

FIGURE 4 | Seasonal changes of mangrove visible vegetation index.

correlated. In general, the RGB vegetation indices were sensitive to meteorological factors, and thus, they could be used to analyze the influence of meteorological conditions on the growth of mangroves.

## 4 DISCUSSION

Machine learning algorithm can improve the segmentation accuracy of mangrove vegetation in aerial RGB images, and



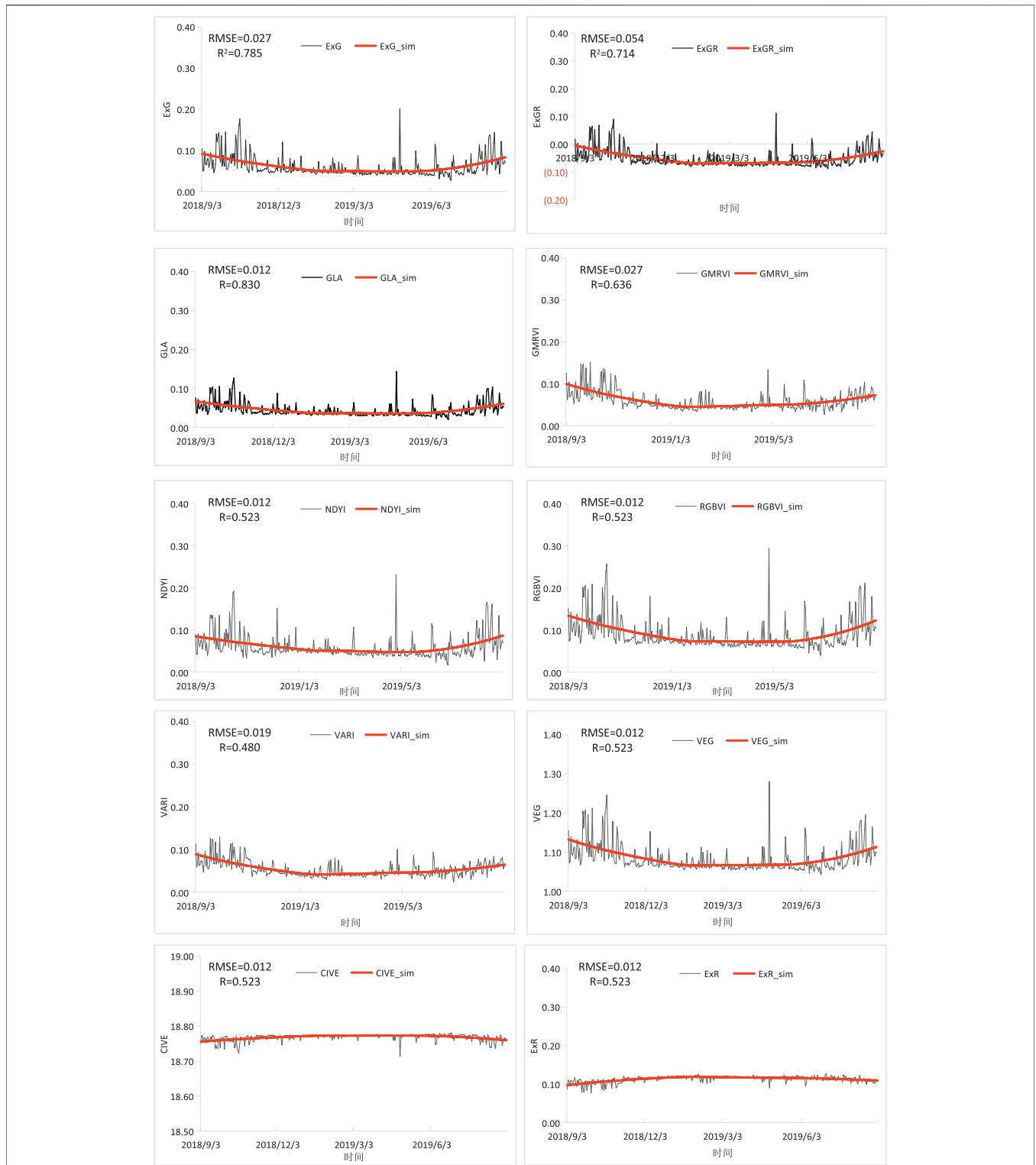


**FIGURE 5 |** Time variations of mangrove RGB vegetation index.

this result has been confirmed in the research on the segmentation of UAV images of mangroves at the park scale (Wen et al., 2020). Digital cameras can be used to monitor the

critical tidal levels of mangrove submersion, and the exposure time of mangroves in the test area is significantly longer than the submerging time (**Figure 4**), which further proved the results of a

**TABLE 3** | Correlation and deviation percentage between fitted and observed values of mangrove RGB vegetation indices.

–	Correlation coefficient/R	Absolute percentage error				
		Spring (%)	Summer (%)	Autumn (%)	Winter (%)	Year (%)
ExG	0.505	15.31	29.92	29.09	12.13	21.60
ExGR	0.555	17.34	30.56	59.66	22.05	31.01
GLA	0.508	15.01	29.26	28.39	11.95	21.14
GMRVI	0.626	13.42	22.18	24.60	14.08	18.54
NDYI	0.430	17.98	39.97	33.76	12.89	26.16
RGBVI	0.503	15.16	29.66	28.53	12.05	21.34
VARI	0.643	12.81	20.02	22.30	14.12	17.29
VEG	0.530	1.11	2.15	2.76	0.93	1.73
CIVE	0.511	0.02	0.04	0.05	0.02	0.03
ExR	0.631	2.46	3.71	7.56	2.75	4.09

**TABLE 4** | Correlation between mangrove RGB vegetation indices and meteorological factors.

–	Daily average temperature	Daily maximum temperature	Daily minimum temperature	Relative humidity	Daily precipitation
NDYI	0.04	0.02	0.02	−0.02	0.14*
GLA	0.11*	0.10	0.09	−0.09	0.11*
VARI	0.26**	0.28**	0.23**	−0.27**	0.03
ExG	0.11*	0.10	0.09	−0.09	0.11*
ExR	−0.27**	−0.29**	−0.23**	0.27**	−0.03
ExGR	0.15**	0.16**	0.13*	−0.14*	0.10
MGRVI	0.24**	0.26**	0.21**	−0.24**	0.05
RGBVI	0.10	0.10	0.08	−0.09	0.11*
NGRDI	0.24**	0.26**	0.21**	−0.24**	0.05
CIVE	−0.11*	−0.11*	−0.09	0.10	−0.11*
VEG	0.14*	0.14*	0.11*	−0.13*	0.11*

Note. ns indicates  $p \geq 0.05$ , \*indicates  $p < 0.05$ , and \*\* indicates  $p < 0.01$ .

**TABLE 5** | Correlation comparison of mangrove RGB vegetation indices.

–	NDYI	GLA	VARI	ExG	ExR	ExGR	MGRVI	RGBVI	NGRDI	CIVE	VEG
NDYI	1.00	0.98	0.70	0.98	−0.68	0.93	0.77	0.98	0.77	−0.97	0.95
GLA	–	1.00	0.84	1.00	−0.82	0.99	0.89	1.00	0.89	−1.00	1.00
VARI	–	–	1.00	0.83	−1.00	0.91	0.99	0.83	0.99	−0.85	0.88
ExG	–	–	–	1.00	−0.82	0.99	0.89	1.00	0.89	−1.00	1.00
ExR	–	–	–	–	1.00	−0.90	−0.99	−0.81	−0.99	0.83	−0.87
ExGR	–	–	–	–	–	1.00	0.95	0.99	0.95	−0.99	1.00
MGRVI	–	–	–	–	–	–	1.00	0.88	1.00	−0.90	0.93
RGBVI	–	–	–	–	–	–	–	1.00	0.88	−1.00	0.99
NGRDI	–	–	–	–	–	–	–	–	1.00	−0.90	0.93
CIVE	–	–	–	–	–	–	–	–	–	1.00	−1.00
VEG	–	–	–	–	–	–	–	–	–	–	1.00

previous research on the seawater submerging rules of mangroves (Zhang and Zheng, 1997; Chen et al., 2006). Under the combined effects of light, precipitation, and seawater submersion, the daily RGB vegetation indices of mangrove vegetation vary greatly, but there is still a significant seasonal trend. However, since the peak time is mostly in autumn, there is a certain difference in the time with peak value of temperature. The day-to-day vegetation indices extracted using visible images vary greatly. The possible reasons are as follows: Mangroves are located in the intertidal zone, and both seawater submersion and extreme weather will have severe impacts on the vegetation indices of

the coastal zone (Wang, 2017), and the digital camera equipped in the ecological station performs automatic exposure and correction according to the light conditions when collecting images, and different exposure times can cause large differences in the quality of vegetation images (Wang et al., 2016).

In this study, we combine image processing with machine learning technology to provide effective technical methods for automatic and continuous monitoring of mangrove vegetation conditions, but there are still many shortcomings. First, limited by the test conditions, the onsite labeling results are used as the references for the evaluation on the accuracy of various

segmentation algorithms, but there is no onsite surveys and sample sampling of the study area. Second, using visual interpretation to determine the submerging status of mangroves can result in low image data processing efficiency. In further research, multispectral cameras equipped to the ground-based and UAV platforms can be used to obtain multispectral and hyperspectral data, and sampling plots can be set in the study area to collect the data related with the physical and chemical properties of plants, so as to enrich the ground data set. Setting camera parameters and improving image correction methods can reduce the variability of RGB vegetation indices. The construction of a prediction model based on the biomass, leaf area index, and chlorophyll content of RGB vegetation indices can provide technical support for real-time, fast, and accurate estimation of mangrove vegetation growth parameters.

## 5 CONCLUSION

The visible images obtained by the ground camera can be used to carry out quantitative monitoring of mangrove growth, which can be achieved by three processes: image screening, vegetation segmentation, and RGB vegetation index calculation.

Image screening can be carried out by using two key indicators: critical tide level and image brightness. The start time of the mangrove submersion in the study area shows a cyclical change with the passage of time, which is delayed first and shifted to an earlier time. On such basis, the average critical tidal level is 334.8 cm in the observation point. The image brightness value is represented by the sum of values of R, G, and B color channels.

Machine learning and NLM filtering are effective strategies to obtain high-precision mangrove segmentation results. The machine learning segmentation algorithm has superiority in the automatic segmentation of mangrove vegetation, and the accuracy of the segmentation results is higher than 80% without filtering. NLM filtering can effectively optimize the segmentation results of various algorithms.

## REFERENCES

- Bendig, J., Yu, K., Aasen, H., Bolten, A., Bennertz, S., Broscheit, J., et al. (2015). Combining UAV-Based Plant Height from Crop Surface Models, Visible, and Near Infrared Vegetation Indices for Biomass Monitoring in Barley. *Int. J. Appl. Earth Observation Geoinformation* 39, 79–87. doi:10.1016/j.jag.2015.02.012
- Campillo, C., Prieto, M. H., Daza, C., Moñino, M. J., and Garcia, M. I. (2008). Using Digital Images to Characterize Canopy Coverage and Light Interception in a Processing Tomato Crop. *horts* 43, 1780–1786. doi:10.21273/hortsci.43.6.1780
- Cao, Q. X. (2017). Remote Sensing Estimation of Mangrove Biomass and Carbon Storage in the Beibu Gulf Coast[J]. *Chin. Acad. For.* 24 (2), 144–149. doi:10.13656/j.cnki.gxkx.20170411.002
- Chen, L., Ding, G. H., and Guo, L. (2011). Image Thresholding Based on Mutual Confirmation of Histogram[J]. *J. Infrared Millimeter Waves* 30 (1), 80–84. doi:10.3724/sp.j.1010.2011.00080

Mangrove RGB vegetation indices include seasonal indices and counterseasonal indices synchronized with temperature changes. Seasonal index VEG and counterseasonal index CIVE can be used as preferred indexes for mangrove growth monitoring. The compound sine function can better simulate the change trend of various RGB vegetation indices, and the simulation effect in winter and spring is better than that in summer and autumn.

The RGB vegetation indices can be used to analyze the effect of meteorological conditions on the growth of mangroves. The RGB vegetation indices of mangroves are sensitive to meteorological factors. Among them, seasonal RGB vegetation indices show positive correlations with average temperature, maximum temperature, minimum temperature, and precipitation, but show negative correlation with relative humidity. On the other hand, the correlations between counterseasonal RGB vegetation indices and the various meteorological factors are opposite to those of the seasonal indices.

## DATA AVAILABILITY STATEMENT

The raw data supporting the conclusions of this article will be made available by the authors, without undue reservation.

## AUTHOR CONTRIBUTIONS

YC wrote the thesis. SF reviewed the manuscript and designed the framework. MS, ZL, LP, WM and CC assisted in the data processing.

## FUNDING

The study is supported by the Open Research Fund Program of Guangxi Key Lab of Mangrove Conservation and Utilization (GKLMC-202004), the Special Project for Climate Change of China Meteorological Administration (CCSF202030), and the Key Project of Fundamental Research Funds (2019Z010).

- Chen, L., Yang, Z., Wang, W., and Lin, P. (2006). Critical Tidal Level for Planting *Kandelia candel* Seedlings in Xiamen. *Ying Yong Sheng Tai Xue Bao* 17 (2), 177–181. doi:10.13287/j.1001-9332.2006.0036
- Chen, M., Zheng, S. F., Liu, X. L., Xu, D. Q., Wang, W., and Kan, H. C. (2017). Cotton Nitrogen Nutrition Diagnosis Based on Digital Image[J]. *J. Agric.* 7 (7), 77–83.
- Gitelson, A. A., Kaufman, Y. J., Stark, R., and Rundquist, D. (2002). Novel Algorithms for Remote Estimation of Vegetation Fraction. *Remote Sensing Environ.* 80 (1), 76–87. doi:10.1016/s0034-4257(01)00289-9
- Guijarro, M., Pajares, G., Riomoros, I., Herrera, P. J., Burgos-Artizzu, X. P., and Ribeiro, A. (2011). Automatic Segmentation of Relevant Textures in Agricultural Images. *Comput. Electron. Agric.* 75 (1), 75–83. doi:10.1016/j.compag.2010.09.013
- Hague, T., Tillett, N. D., and Wheeler, H. (2006). Automated Crop and Weed Monitoring in Widely Spaced Cereals. *Precision Agric.* 7 (1), 21–32. doi:10.1007/s11119-005-6787-1

- Han, D., Wu, H. J., Ma, Z. Y., Han, G. D., Wu, P., and Zhang, Q. (2019). Feature Extraction and Recognition of Typical Pastures in Grassland[J]. *Chin. J. Grassland* 41 (4), 128–135. doi:10.16742/j.zgdx.20190043
- Jones, A. R., Segaran, R. R., Clarke, K. D., Waycott, M., Goh, S. H., Gillanders, B. M., et al. (2020). Estimating Mangrove Tree Biomass and Carbon Content: a Comparison of forest Inventory Techniques and Drone Imagery[J]. *Front. Mar. Sci.* 6, 13. doi:10.3389/fmars.2019.00784
- Kataoka, T., Kaneko, T., Okamoto, H., and Hata, S. (2003). “Crop Growth Estimation System Using Machine Vision[J].” in IEEE/ASME International Conference on Advanced Intelligent Mechatronics, Kobe, Japan, 20–24 July 2003 (IEEE), b1079–b1083.
- Kovacs, J. M., Wang, J., and Flores-Verdugo, F. (2005). Mapping Mangrove Leaf Area Index at the Species Level Using IKONOS and LAI-2000 Sensors for the Agua Brava Lagoon, Mexican Pacific. *Estuarine, Coastal Shelf Sci.* 62, 377–384. doi:10.1016/j.ecss.2004.09.027
- Li, J., Jiang, N., Baoyin, B. T., Zhang, F., Zhang, W. J., and Wang, W. (2020). Spatial Color Clustering Algorithm and its Application in Image Feature Extraction[J]. *J. Jilin Univ. (Science Edition)* 58 (3), 627–633. doi:10.13413/j.cnki.jdxblx.2019282
- Liu, S. Y., Li, L., Te, R. G., Li, Z. Q., Ma, J. Y., and Zhu, R. F. (2021). Threshold Segmentation Algorithm Based on Histogram Area Growing for Remote Sensing Images[J]. *Bull. Surv. Mapp.* (2), 25–29. doi:10.13474/j.cnki.11-2246.2021.0037
- Liu, Z. P., Kuang, S. W., Ma, R. S., Wu, X. K., Wang, D., Li, L., et al. (2020). Study on Automatic Recognition Technology of Sugarcane Emergence Stage Based on Image Features[J]. *Sugarcane and Canesugar* 49 (5), 41–46.
- Lu, M., Shen, S. H., Wang, C. Y., and Li, M. S. (2011). Initial Exploration of maize Phenological Stage Based on Image Recognition[J]. *Chin. J. Agrometeorology* 32 (3), 423–429. doi:10.3969/j.issn.1000-6362.2011.03.017
- Ma, B. Y., Liu, C. N., Gao, M. F., Ban, X. J., Huang, H. Y., Wang, H., et al. (2020). Region Aware Image Segmentation for Polycrystalline Micrographic Image Using Deep Learning[J]. *Chin. J. Stereology Image Anal.* 25 (2), 120–127. doi:10.13505/j.1007-1482.2020.25.02.004
- Ma, X., Qi, L., and Zhang, X. C. (2008). Segmentation Technology of *Exserochilum Turcicum* Image Based on Fuzzy Clustering Analysis[J]. *J. Agric. Mechanization Res.* (12), 24–26. doi:10.3969/j.issn.1003-188X.2008.12.007
- Meyer, G. E., Hindman, T. W., and Laksmi, K. (1999). Machine Vision Detection Parameters for Plant Species Identification[J]. *Precision Agric. Biol. Qual.* 327–335. doi:10.1117/12.336896
- Min, L., Gao, K., Li, W., Wang, H., Li, T., Wu, Q., et al. (2020). A Review of Optical Remote Sensing Image Segmentation Technology[J]. *Spacecraft Recovery & Remote Sensing* 41 (6), 1–13. doi:10.3969/j.issn.1009-8518.2020.06.001
- Ostu, N. (1979). A Threshold Selection Method from gray-level Histograms[J]. *IEEE Trans. Syst. Man Cybernetics* 9 (1), 62–66. doi:10.1109/tsmc.1979.4310076
- Pérez, A. J., López, F., Benlloch, J. V., and Christensen, S. (2000). Colour and Shape Analysis Techniques for weed Detection in Cereal fields. *Comput. Electron. Agric.* 25 (3), 197–212. doi:10.1016/s0168-1699(99)00068-x
- Peter, J., Hogland, J., Hebblewhite, M., Hurley, M., Hupp, N., and Proffitt, K. (2018). Linking Phenological Indices from Digital Cameras in Idaho and Montana to MODIS NDVI. *Remote Sensing* 10, 1612. doi:10.3390/rs10101612
- Purcell, L. C. (2000). Soybean Canopy Coverage and Light Interception Measurements Using Digital Imagery. *Crop Sci.* 40, 834–837. doi:10.2135/cropsci2000.403834x
- Ramsey, E. W., and Jensen, J. R. (1996). Remote Sensing of Mangrove Wetlands: Relating Canopy Spectra to Site-specific Data[J]. *Photogrammetric Eng. Remote Sensing* 62 (31), 939–948.
- Ren, J., Li, Z. N., and Fu, Y. P. (2004). Edge Detection of Color Images Based on Wavelet and Reduced Dimensionality Model of RGB[J]. *J. Zhejiang Univ. (Engineering Science)* 38 (7), 856–859+892. doi:10.3785/j.issn.1008-973X.2004.07.014
- Shi, P. H., Wang, Y., Yuan, Z. Q., Sun, Q. Y., Cai, S. Y., and Lu, X. Z. (2020). Winter Wheat Nitrogen Nutrition Index Based on Canopy RGB Image[J]. *J. Nanjing Agric. Univ.* 43 (5), 829–837. doi:10.7685/jnau.202001020
- Sulik, J. J., and Long, D. S. (2016). Spectral Considerations for Modeling Yield of Canola. *Remote Sensing Environ.* 184, 161–174. doi:10.1016/j.rse.2016.06.016
- Wang, C. Y., Guo, X. Y., Wen, W. L., Du, J. J., and Xiao, B. X. (2016). Application of Hemispherical Photography on Analysis of maize Canopy Structural Parameters under Natural Light[J]. *Trans. Chin. Soc. Agric. Eng.* 32 (4), 157–162. doi:10.11975/j.issn.1002-6819.2016.04.022
- Wang, X. L. (2017). Spatiotemporal Variations of Extreme Climate Events and Their Impacts on NDVI in Coastal Area of China[D]. University of Chinese Academy of Sciences. Doctoral dissertation
- Wen, X., Jia, M. M., Li, X. Y., Wang, Z. M., Zhong, C. R., and Feng, E. H. (2020). Recognition of Mangrove Canopy Species Based on Visible Unmanned Aerial Vehicle Images[J]. *J. For. Environ.* 40 (5), 486–496. doi:10.13324/j.cnki.jfcf.2020.05.005
- Woebbecke, D. M., G. E. Meyer, G. E., K. Von Bargen, K. V., and Mortensen, D. A. (1995). Color Indices for Weed Identification under Various Soil, Residue, and Lighting Conditions. *Trans. Asae* 38 (1), 259–269. doi:10.13031/2013.27838
- Wu, L. F., Wang, M. G., Fu, H., and Jian, M. (2018). Automatic Recognition of Cotton Growth by Combining Deep Learning Based Object Recognition and Image Classification[J]. *Chin. Sci. Technol. Paper* 13 (20), 2309–2316. doi:10.3969/j.issn.2095-2783.2018.20.005
- Wu, Q. (2014). *Research on Automatic Detection of Cotton Growth Stages by Image Processing technology[D]*. Hubei: Huazhong University of Science and Technology.
- Yan, C., Sun, Z. Q., Tin, E. G., Zhao, Y. Y., and Fan, X. Y. (2021). Research Progress of Medical Image Segmentation Based on Deep Learning [J]. *Electron. Sci. Technol.* 34 (2), 7–11. doi:10.16180/j.cnki.issn1007-7820.2021.02.002
- Yang, H., Zhao, J., Lan, Y., Lu, L., and Li, Z. (2018). Fraction Vegetation Cover Extraction of winter Wheat Based on RGB Image Obtained by UAV. *Int. J. Precision Agric. Aviation* 1 (1), 54–61. doi:10.33440/j.ijpaa.20190202.44
- Zhang, Q. M., and Zheng, D. Z. (1997). The Relationship between Mangrove Zone and Tidal Flats and Tidal Levels[J]. *Acta Ecologica Sinica* 17 (3), 258–265.
- Zhang, W. (2016). Monitoring the Areal Variation of Mangrove in Beibu Gulf Coast of Guangxi China with Remote Sensing Data[J]. *J. Guangxi Univ. (Natural Sci. Edition)* 40 (6), 1570–1576. doi:10.13624/j.cnki.issn.1001-7445.2015.1570
- Zhou, H. J., Liu, Y. D., Fu, J. D., Sui, F. G., and Zhu, R. X. (2015). Analysis of maize Growth and Nitrogen Nutrition Status Based on Digital Camera Images[J]. *J. Qingdao Agric. Univ. (Natural Sci. Edition)* 32 (1), 1–7. doi:10.3969/j.issn.1674-148X.2015.01.001
- Zhu, Y. H., Liu, L., Liu, K., Wang, S. G., and Ai, B. (2014). Progress in Researches on Plant Biomass of Mangrove Forests[J]. *Wetland Sci.* 12 (4), 515–526. doi:10.13248/j.cnki.wetlandsci.2014.04.016
- Zhu, Y., Liu, K., Myint, S. W., Du, Z., Li, Y., Cao, J., et al. (2020). Integration of GF2 Optical, GF3 SAR, and UAV Data for Estimating Aboveground Biomass of China’s Largest Artificially Planted Mangroves. *Remote Sensing* 12 (12), 2039. doi:10.3390/rs12122039

**Conflict of Interest:** The authors declare that the research was conducted in the absence of any commercial or financial relationships that could be construed as a potential conflict of interest.

**Publisher’s Note:** All claims expressed in this article are solely those of the authors and do not necessarily represent those of their affiliated organizations, or those of the publisher, the editors, and the reviewers. Any product that may be evaluated in this article, or claim that may be made by its manufacturer, is not guaranteed or endorsed by the publisher.

Copyright © 2022 Chen, Fang, Sun, Liu, Pan, Mo and Chen. This is an open-access article distributed under the terms of the Creative Commons Attribution License (CC BY). The use, distribution or reproduction in other forums is permitted, provided the original author(s) and the copyright owner(s) are credited and that the original publication in this journal is cited, in accordance with accepted academic practice. No use, distribution or reproduction is permitted which does not comply with these terms.